Deep Learning-Tuned Adaptive Inertia Weight in Particle Swarm Optimization for Medical Image Registration

Katharina Krämer[1][a], Stefan Müller[1] and Michael Kosterhon[2]
[1]*Institute of Computervisualistics, University of Koblenz, Universitätsstraße 1, 56070 Koblenz, Germany*
[2]*Medical Center Johannes Gutenberg University, Langenbeckstraße 1, 55131 Mainz, Germany*
{kkraemer, stefanm}@uni-koblenz.de, mikoster@uni-mainz.de

Keywords: Spondylodesis Surgery, Medical Image Registration, Particle Swarm Optimization, Deep Learning, Parameter Optimization, Benchmark Functions, Search Space Volume.

Abstract: A novel parameter training approach for Adaptive Inertia Weight Particle Swarm Optimization (AIW-PSO) using Deep Learning is proposed. In PSO, balancing exploration and exploitation is crucial, with inertia governing parameter space sampling. This work presents a method for training transfer function parameters that adjust the inertia weight based on a particle's individual search ability (ISA) in each dimension. A neural network is used to train the parameters of this transfer function, which then maps the ISA value to a new inertia weight. During inference, the best possible success ratio and lowest average error are used as network inputs to predict optimal parameters. Interestingly, the parameters across different objective functions are similar and assume values that may appear spatially implausible, yet outperform all other considered value expressions. We evaluate the proposed method Deep Learning-Tuned Adaptive Inertia Weight (TAIW) against three inertia strategies: Constant Inertia Strategy (CIS), Linear Decreasing Inertia (LDI), Adaptive Inertia Weight (AIW) on three benchmark functions. Additionally, we apply these PSO inertia strategies to medical image registration, utilizing digitally reconstructed radiographs (DRRs). The results show promising improvements in alignment accuracy using TAIW. Finally, we introduce a metric that assesses search effectiveness based on multidimensional search space volumes.

1 INTRODUCTION

The Particle Swarm Optimization (PSO) is an established method for solving optimization problems across various fields. One of the central challenges in applying PSO is achieving a balance between exploration and exploitation in the search process. This balance is significantly influenced by the inertia weight, which dominates the dynamics of particle movement. Traditionally, different strategies for inertia have been proposed, including constant, linearly decreasing or even chaotic values. However, these methods do not demonstrate optimal performance across various applications. Consequently, researchers have developed adaptive approaches to dynamically adjust the inertia weight according to the requirements of the search process. The advancement of these adaptive strategies through the incorporation of deep learning techniques represents a promising step towards enhancing PSO performance and improving efficiency. In this work, we propose a novel approach based on deep learning that dynamically adjusts the inertia parameters for each particle. As an outlook we propose a metric that evaluates the success probability based on search space volumes. Our objective is to demonstrate the advantages of this AI-supported method through benchmark functions and the registration of medical images.

[a] https://orcid.org/0009-0003-1965-7512

2 RELATED WORK

2.1 Medical Context

Medical image registration is essential in healthcare, aligning images from various modalities like CT, MRI, and X-ray to provide a comprehensive view of a patient's anatomy. This process is crucial for applications such as surgical assistance, disease diagnosis, and treatment planning. PSO has become a reliable tool for finding the appropriate transformations

Krämer, K., Müller, S. and Kosterhon, M.
Deep Learning-Tuned Adaptive Inertia Weight in Particle Swarm Optimization for Medical Image Registration.
DOI: 10.5220/0013122000003912
Paper published under CC license (CC BY-NC-ND 4.0)
In *Proceedings of the 20th International Joint Conference on Computer Vision, Imaging and Computer Graphics Theory and Applications (VISIGRAPP 2025) - Volume 3: VISAPP*, pages 307-318
ISBN: 978-989-758-728-3; ISSN: 2184-4321
Proceedings Copyright © 2025 by SCITEPRESS – Science and Technology Publications, Lda.

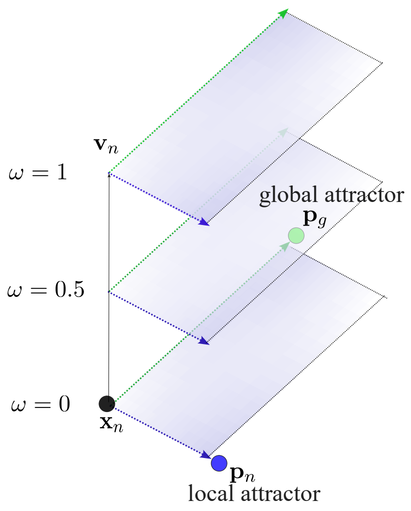

Figure 1: Impact of different ω values on PSO search area.

in medical image registration, effectively optimizing multi-dimensional parameter spaces. A recent review by (Ballerini, 2024) examines 24 studies utilizing PSO in this area. Two papers focus on the registration of a computed tomography volume (CT) with two X-ray images. (Zaman and Ko, 2018) showed that PSO is better suited for this problem than gradient-based methods, such as Momentum Stochastic Gradient Descent (MSGD) or Nesterov Accelerated Gradient (NAG), as these methods are more prone to getting trapped in local optima. Furthermore, (Yoon et al., 2021) developed a multi-threaded approach, enabling real-time registration, which highlights the potential of PSO for practical applications in the medical field.

2.2 Particle Swarm Optimization

The Particle swarm optimization, developed by (Kennedy and Eberhart, 1995), is a swarm-based search algorithm that optimizes an objective function by selecting global and local attractors in each iteration to locate a global optimum. Each particle is influenced both by the social behavior of the swarm and its own personal experience. Movement $\mathbf{v}$ of the n-th particle is calculated by:

$$\mathbf{v}_n \leftarrow \omega \mathbf{v}_n + c_1 r_1 (\mathbf{p}_n - \mathbf{x}_n) + c_2 r_2 (\mathbf{p}_g - \mathbf{x}_n) \quad (1)$$

Inertia weight ω controls the influence of a particle's previous velocity $\mathbf{v}_n$ on its current movement. Local and global attractors also guide the particle: the local one directs it from its current position $\mathbf{x}_n$ toward its personal best $\mathbf{p}_n$, and the global one from $\mathbf{x}_n$ toward the global best $\mathbf{p}_g$. The magnitude of these components is scaled by randomly chosen factors $r_1 \in [0,1]$ and $r_2 \in [0,1]$. The new particle position is $\mathbf{x}_n \leftarrow \mathbf{x}_n + \mathbf{v}_n$. In the version of PSO used in this paper, not all particles converge at one point, but the number of iterations is fixed. The success of the search depends on the parameterization of ω, c_1, and c_2. Typically, $c_1 = c_2$ is set in a range of $[1.5, 2]$ as in e.g. (Lu et al., 2023), (Kessentini and Barchiesi, 2015) or (Shi and Eberhart, 1998). This is done to balance the cognitive component effecting a global sampling (exploration) and the social component that drives convergence (exploitation). Within our work c_1 decreases linearly from 1.5 to 0 and c_2 increases from 0 to 1.5, reflecting the need for stronger exploration at the start and greater exploitation towards the end of the search. Focusing only on the social and cognitive components would oversimplify the complexities of the optimization problem.

The inertia parameter ω introduces an additional layer of control by physically mimicking the behavior of individual particles in the swarm. ω plays a crucial role in shaping the search behavior, as discussed by (Wang et al., 2018), (Mirjalili et al., 2020) and (Shi and Eberhart, 1998). A higher value encourages particles to explore more broadly. This helps avoiding premature convergence to local optima by exploring diverse regions of the search space. Conversely, a lower inertia weight focuses the search around promising areas, enhancing the exploitation of known good solutions.

As shown in Figure 1, different values of ω lead to distinct search regions in worst case scenario if $\mathbf{v}_n$ is linearly independent of $\mathbf{p}_g - \mathbf{x}_n$ and $\mathbf{p}_n - \mathbf{x}_n$. This illustrates how varying the inertia weight can influence the algorithm's exploration of the solution space and underscores the potential for adaptive inertia strategies to improve PSO performance. Numerous methods have aimed to enhance search performance in PSO. A simple approach is to keep ω constant at 1, ensuring good exploration but often struggling with convergence. A more advanced strategy involves adjusting ω over iterations; for example, (Shi and Eberhart, 1998) proposed a version where ω decreases linearly. (Bansal et al., 2011) found that among simple strategies, those using random inertia values were particularly effective, highlighting the potential for adaptive methods.

AIW-PSO (Qin et al., 2006) introduced a basic adaptive approach that dynamically adjusts ω based on the fitness value of each particle, mapping it to a new inertia value through a transfer function. The mapping adjusts between exploration and exploitation, where a lower fitness value encourages exploration and a higher value promotes exploitation, thus balancing the search strategy. Our method, TAIW-PSO, enhances this by employing a neural network for better selection of inertia values.

Additionally, (Kessentini and Barchiesi, 2015) proposed increasing ω when particles become too close, promoting exploration while controlling convergence. Non-parametric PSO (Beheshti and Shamsuddin, 2015) takes a different approach by dynamically adjusting particle neighborhoods, initially limiting influence to local neighbors and gradually expanding to include all particles by the end of the search. PSO is frequently used to optimize neural networks, particularly for backpropagation, as shown in (Zhou et al., 2024). Conversely, the use of deep learning to enhance PSO parameters such as the inertia weight ω is less common and has emerged only in recent years. Several approaches have adjusted PSO parameters using Reinforcement Learning (RL). For instance, (Liu et al., 2019) propose an adaptive control algorithm for PSO based on Q-learning, where a policy network allows an agent to select optimal actions to maximize long-term rewards. This method uses a three-dimensional Q-table to assign actions based on particle states. However, it is limited to only four fixed states, restricting the variety of parameter configurations that may not suffice for all particle scenarios.

A survey by (Song et al., 2024) highlights the increase in studies focusing on reinforcement learning, particularly Q-learning, over the past three years. Among these, three notable papers enhance PSO: (Gao et al., 2023) presents an opposition-based learning strategy to prioritize alternative objectives avoiding premature convergence; (Li et al., 2023) introduce a PSO variant with a neighborhood differential mutation strategy and a dynamic oscillation inertial weight; and (Yin et al., 2023) emphasizes adjusting all parameters using a reward system based on observed improvements. While this last approach avoids fixed parameter values, the complexity of estimating all three parameters simultaneously poses significant challenges. Training a neural network to understand the combined effects of multiple parameters can complicate the training process and the interpretability of the results. According to (Haarnoja et al., 2018), RL presents several challenges, especially when managing complex state spaces. RL models are often tailored to specific environments or tasks, making it difficult to generalize learned strategies to new or altered situations. This limitation can be problematic in unpredictable environments, as the adaptive capabilities of these algorithms may become restricted. Additionally, extensive training is often necessary for each specific application, which can be resource-intensive and typically requires substantial data and computational resources.

Given these challenges, we chose not to adopt another RL approach, opting instead for a more fundamental strategy to approach the optimization problem while still leveraging the advantages of deep learning technologies. For instance, the study by (Pawan et al., 2022) demonstrates a different application of deep learning in enhancing the PSO strategy, focusing on directly training the inertia parameter ω based on the particles' search capabilities. Their methodology evaluates each particle's behavior using Convolutional Neural Networks (CNNs) and Long Short-Term Memory networks (LSTMs). In contrast, our approach simplifies this process by learning the transfer function proposed by (Qin et al., 2006), which maps the individual search ability of each particle to a new inertia value. This makes our method less dependent on training data while still utilizing the strengths of classical methods and deep learning combined.

In comparing strategies, we followed a similar approach to (Pawan et al., 2022), starting with the Constant Inertia Strategy (CIS), where $\omega = 1$, then progressing to the Linear Decreasing Inertia (LDI) strategy, where ω decreases from 1 to 0 as proposed by (Shi and Eberhart, 1998), and finally to AIW-PSO (Qin et al., 2006), serving as the foundation for our Deep Learning-Tuned AIW-PSO (TAIW).

3 BENCHMARK FUNCTIONS

The comparison is made with the help of three established benchmark functions (Qin et al., 2006): Rastrigin function $f(x)$, Griewank function $g(x)$ and Rosenbrock function $h(x)$, where $\mathbf{x}$ is a n-dimensional vector.

$$f(\mathbf{x}) = 10n + \sum_{i=1}^{n} \left[x_i^2 - 10\cos(2\pi x_i)\right] \tag{2}$$

$$g(\mathbf{x}) = 1 + \frac{1}{4000}\sum_{i=1}^{n} x_i^2 - \prod_{i=1}^{n}\cos\left(\frac{x_i}{\sqrt{i}}\right) \tag{3}$$

$$h(\mathbf{x}) = \sum_{i=1}^{n-1}\left[100\cdot(x_{i+1} - x_i^2)^2 + (1 - x_i)^2\right] \tag{4}$$

These functions are examined in six dimensions, as the application problem considered in Section 6 is also 6-dimensional, which makes the results more comparable for the problem complexity of interest. They were selected based on their differences in local optima to examine a diverse range of scenarios.

4 INERTIA ADJUSTMENT

(Qin et al., 2006) developed a metric depicting the individual search ability ISA_{n_i} of a single particle n in

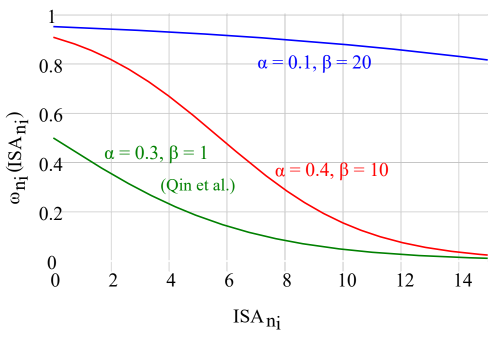

Figure 2: Possible transfer functions mapping *ISA* on ω.

dimension i with $\varepsilon > 0$:

$$ISA_{n_i} = \frac{|x_{n_i} - p_{n_i}|}{|p_{n_i} - p_{g_i}| + \varepsilon} \quad (5)$$

A high ISA value indicates the particle is far from its personal best and exploring new regions, while a low ISA value suggests the particle is close to its personal best or its best is far from the global optimum. To update ω accordingly, *ISA* is used in a transfer function:

$$\omega_{n_i}(ISA_{n_i}) = 1 - \frac{1}{1 + e^{-\alpha ISA_{n_i}}} \quad (6)$$

We opted to adjust the formula presented in (Qin et al., 2006) to Equation (6) due to the ambiguous information in their paper. We had to decide between relying on the formula or the graph describing the transfer function in their work. The description of the impact of α on ω led us to conclude that the graph contained the accurate information that goes along with the authors' intention. (Bansal et al., 2011) show that an adaptive inertia strategy does not necessarily perform better than a rudimentary approach. Whether exploration and exploitation are successfully balanced depends strongly on the parameterization of the trasfer function. (Qin et al., 2006) have tested several values for α, but using transfer function Equation (6), the inertia can never become larger than 0.5, which has a negative impact on exploration. (Shi and Eberhart, 1998) state that ω should be within range $[0.8, 1.2]$ to effectively find the global optimum. If it is smaller than 0.8 the search is dominated by exploitation and the result of the search gets more random, converging to local minima. Therefore, we added parameter β to Equation (6):

$$\omega_{n_i}(ISA_{n_i}) = 1 - \frac{1}{1 + \beta e^{-\alpha ISA_{n_i}}} \quad (7)$$

This makes it possible to enable values of ω between 1 and 0, with different slopes, as illustrated in Figure 2. To find the best parameters (α, β) for Equation (7) we set up a neural network that models the

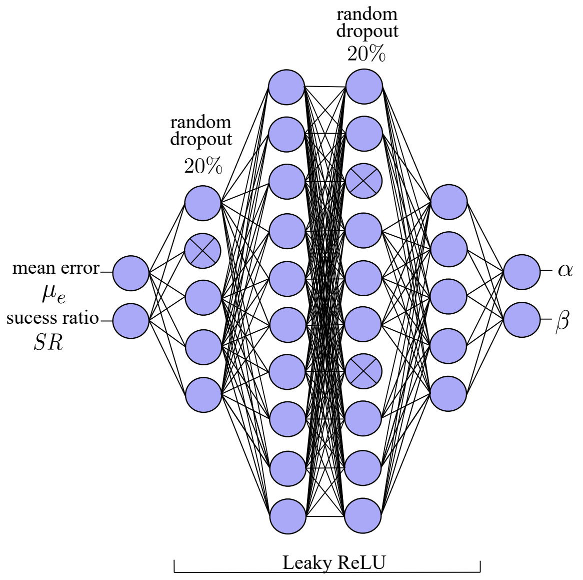

Figure 3: Network architecture: fully connected layers of shape (2-5-10-10-5-2), dropout 20%, activation function of hidden layers: Leaky ReLU.

relationship between these parameters and the evaluation metrics (μ_e, SR) (cf. Figure 3). These metrics are based on 100 test runs of the PSO with the respective transfer function parameters α and β. From the results, the average error μ_e and a success ratio SR were calculated. A run is considered successful if the error value falls below a threshold of 0.05. In the inference step the best possible metric-pair $(0, 1)$ is given as an input and the output will be the optimal parameters based on the training data, that is generated for each objective function. Our approach progressively doubling and halving the number of neurons between layers facilitates a hierarchical feature extraction process, enabling the network to learn and represent different levels of features (Bengio, 2009).

Lastly, we chose a total number of 30 hidden neurons. Mean Squared Error was chosen as the metric for backpropagation, Adam as the optimizer (Kingma, 2014) and a learning rate of 0.001, as well as 300 epochs and a batch size of 8. These parameters were found by trial and error, aiming to effectively reduce the loss. The training dataset consists of 900 samples (α, β), with $\alpha \in [0.1, 0.4]$ and $\beta \in [1, 20]$ uniformly distributed, for which the PSO is run 100 times each. These runs can then be used to calculate (μ_e, SR), which then serve as the network input. After the input layer, all values are normalized to ensure consistent scaling. An attempt was also made to include the variance as a third input parameter. However, this has led to a deterioration in generalizability. Additionally, a 20% dropout was introduced because the validation loss was consistently higher than the

Table 1: Comparison of Error Variance: Mean vs. Weighted Mean Across Different Iteration Counts; Iter. = Iterations.

	Iter.	PSO test runs										σ^2
μ_e	100	439.1	260.1	10038.4	761.4	948	221.5	474	657.5	259.9	274	9,200,804
	500	329.2	449.2	2,460.4	290.8	521.5	452.6	528.3	466.5	356.3	429.7	420,430
$\overline{\mu_e}$	100	44	40.99	16.68	69.32	74.96	30.13	64.85	65.06	33.83	54.42	371
	500	41.87	49.38	52.78	47.79	51.58	51.45	54.85	56.13	45.94	47.79	18.4
SR	100	0.55	0.49	0.66	0.53	0.56	0.66	0.49	0.5	0.68	0.54	0.0054
	500	0.58	0.56	0.554	0.592	0.52	0.55	0.578	0.556	0.56	0.55	0.0004

training loss, which indicates overfitting.

The issue with the training data is that the network can only be trained effectively if the parameters consistently produce the same error values during the PSO execution. However, μ_e is sensitive to outliers, which increases its variance. Training on values with high variance would lead to arbitrary results. The solution to this problem is to use the weighted mean $\overline{\mu_e}$ instead:

$$\overline{\mu_e} = \frac{\sum(x \cdot \overline{f}_{kde}(x))}{\sum \overline{f}_{kde}(x)} \tag{8}$$

Kernel density estimation (KDE) was used to estimate the probability density function $\overline{f}_{kde}$ of PSO runs based on a smooth approximation to the distribution of the data. For data generation 400 runs for each objective function with one single distribution were generated. Actually, KDE would have to be performed for each parameter pair of the training data set, but that would be very time-consuming and the exact magnitude of f_{kde} makes little difference. The fixed probability distribution, centered around the optimum, focuses the network on this region, leading to lower variance. As a result, the network concentrates more on the nuances between better parameters. These parameters stand out more clearly because the noise is minimal.

Several tests evaluating the performance of μ_e and $\overline{\mu}_e$ were then conducted using the Rosenbrock function ($h(x)$), with 10 sets of 100 runs each and parameters ($\alpha = 0.1, \beta = 1$) (cf. Table 1). From these, mean μ_e, weighted mean $\overline{\mu_e}$ and success ratio *SR* were calculated based on the same runs. At first, the variance decreases with an increasing number of iterations. For instance, increasing the iterations from 100 to 500 resulted in the variance dropping to 4.5% (μ_e), 7.3% (*SR*), and 4.9% ($\overline{\mu_e}$). However, the number of iterations used in training must match the number used in the actual application of PSO, which cannot be arbitrarily high due to time constraints. When comparing the mean to the weighted mean, several important differences emerge. The mean is highly susceptible to outliers, which can skew the results significantly, especially in datasets containing extreme values. In contrast, the weighted mean proves to be more stable, as the weighting helps to reduce the influence of less frequent or extreme values, providing a more accurate representation of the data's central tendency.

Table 2: Loss values across folds for Cascade and Regular Training for optimizing Rastrigin function $f(x)$; TL= Training Loss; VL= Validation Loss.

	Cascade		Regular	
Fold	TL	VL	TL	VL
0	2.132	1.858	2.183	1.821
1	1.663	1.204	1.96	1.51
2	1.403	3.093	1.869	2.868
3	1.503	1.453	2.06	1.743
4	1.436	1.832	1.991	2.159
Average	1.627	1.888	2.013	2.02

For the training process we developed a modified version of the traditional cross-validation (Berrar et al., 2019), which can be described as a cascading training. Instead of training multiple models and selecting the best one, this approach involves continuously training a single model across different data folds. As the model sees new sections of the data progressively, it continuously improves, rather than being reset after each fold. Table 2 shows the results of the Cascade training and regular training across five folds. As can be seen, the Cascade approach achieves a lower average training loss and validation loss. These results suggest that the Cascade training strategy leads to better adaptation to the training data and generalization indicated by the lower validation loss. This occurs because the model incrementally learns from the entire dataset without being reset, with the training gradually adapting to the data fold by fold. The range for the desired parameters (α, β) was initially unclear when creating the training dataset. During the neural network's initial training, it was found that β could take negative values, with output parameters for the Rosenbrock function being $[0.5641866, -0.6367712]$. This leads to a hyperbola for the transfer function, where only the positive range is relevant, as $ISA \geq 0$. The hyperbola is adjusted by the parameters so that ω falls within $[-1.747, 0)$, causing particles to move in the opposite direction of their previous trajectories. To enhance results, the training data was refined to $\alpha \in [0.4, 1]$ and $\beta \in [-1, 0]$.

Table 3: Evaluation of benchmark functions $h(x)$, $g(x)$ and $f(x)$ that are optimized by different PSO inertia strategies namely LDI, CIS and AIW with different transfer functions that can be seen in Figure 2; evaluation metrics are mean μ_e and success ratio *SR* with tolerance threshold 0.05; Each plot depicts the iterations versus the logarithmized error for better visibility.

PSO	Rosenbrock function $h(x)$	Griewank function $g(x)$	Rastrigin function $f(x)$
LDI	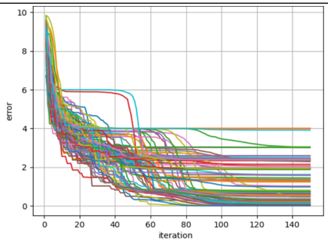 μ_e 703.223, *SR* 0.11	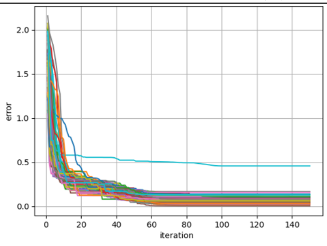 μ_e 0.194, *SR* 0.02	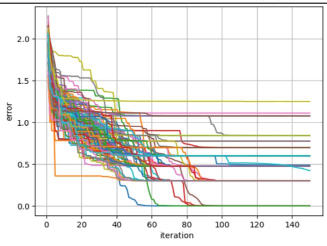 μ_e 2.961, *SR* 0.05
CIS	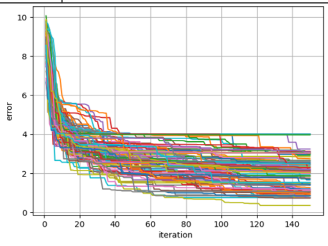 μ_e 963.6, *SR* 0	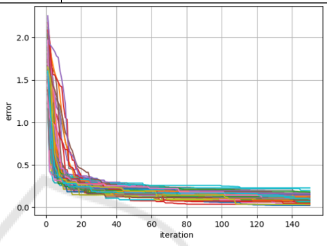 μ_e 0.288, *SR* 0	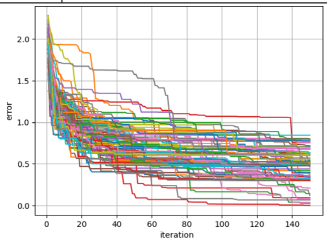 μ_e 2.162, *SR* 0.01
AIW α= 0.3 β = 1	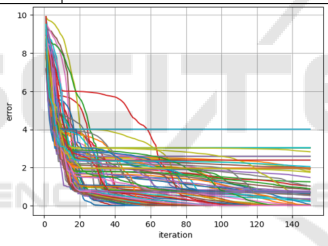 μ_e 394.388, *SR* 0.41	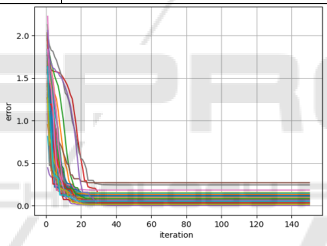 μ_e 0.149, *SR* 0.18	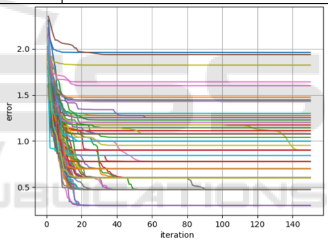 μ_e 9.77, *SR* 0
AIW α= 0.1 β = 20	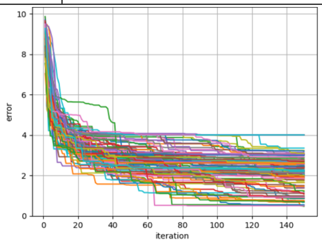 μ_e 715.671, *SR* 0	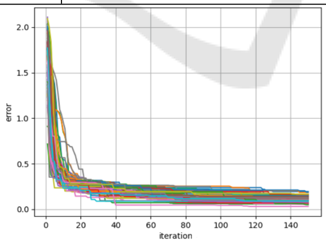 μ_e 0.277, *SR* 0	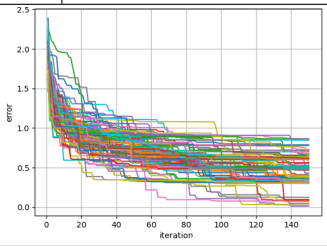 μ_e 2.178, *SR* 0.01
AIW α= 0.4 β = 10	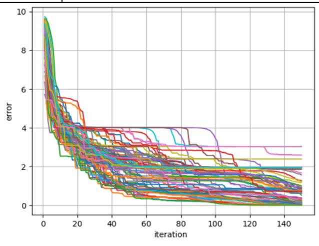 μ_e 60.64, *SR* 0.15	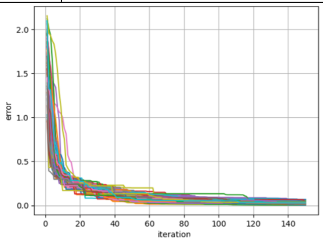 μ_e 0.068, *SR* 0.31	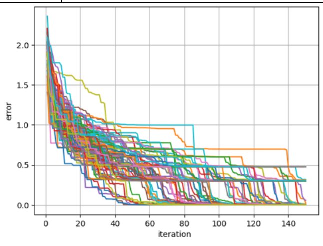 μ_e 0.363, *SR* 0.65

Table 4: Evaluation of benchmark functions $h(x)$, $g(x)$ and $f(x)$ that are optimized by TAIW-PSO where α and β are computed by the neural network; evaluation metrics are weighted mean $\overline{\mu}_e$ and success ratio SR with tolerance threshold 0.05.

PSO	Rosenbrock function $h(x)$	Griewank function $g(x)$	Rastrigin function $f(x)$
TAIW	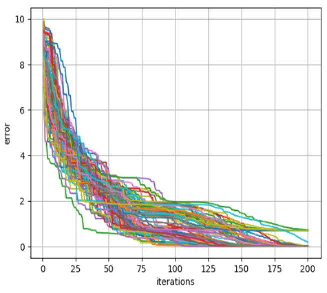	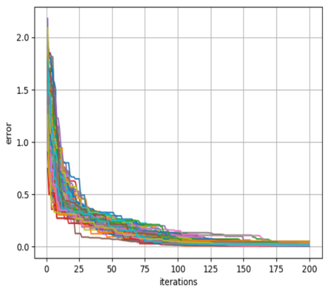	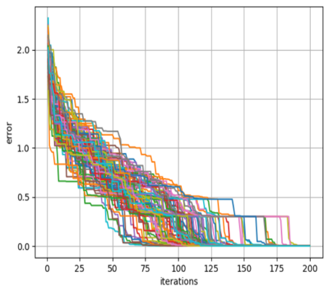
(α,β)	(0.793, -0.793)	(0.627, -0.864)	(0.81, -0.975)
$\overline{\mu}_e$	0.457	0.051	12×10^{-6}
SR	0.83	0.54	1

Table 5: Mean loss and loss variance for different models m (Rastrigin function $f(x)$).

m	Loss	σ^2	(α,β)	$(\overline{\mu_e}, SR)$
1	1.522	25.62	(0.68, -1.05)	(0.24, 0.58)
2	1.604	25.76	(0.37, -0.31)	(12.7, 0)
3	1.582	25.53	(0.81, -0.98)	$(12\times10^{-6}, 1)$
4	1.551	26.45	(0.64, -0.92)	(0.01, 0.89)
5	1.524	24.84	(0.76, -0.68)	(0.26, 0.67)

5 EXPERIMENTS AND EVALUATION

To evaluate model performance, we consider the mean average loss and variance of the loss values. A low mean loss indicates good predictions, while variance reflects the consistency of model performance.

However, these metrics did not reliably indicate the model's effectiveness in capturing underlying data patterns, as they did not correlate strongly with the quality of outputs generated by the PSO process. Our approach focused on training multiple models and evaluating their outputs with the PSO algorithm, emphasizing outcomes over loss and variance σ^2. Table 5 presents the evaluation of five models trained for the Rastrigin function. Notably, the parameters of Model 3 yield the best results with $(\overline{\mu_e}, SR) = (12\times10^{-6}, 1)$ almost reaching the ideal of $(0,1)$, even though it does not have the lowest loss and variance values. This underscores that low loss and variance values do not necessarily correlate with the best parameter outcomes. This trend is consistent across the other benchmark functions evaluated in this study.

First, the methods CIS, LDI, and three AIW example cases of the transfer functions (as seen in Figure 2) will be examined using the PSO to optimize $f(x)$, $g(x)$ and $h(x)$. The results are depicted in Table 3. Each of the plotted 100 curves describes the course of a PSO search process, that is performed by 1000 particles, showing the best logarithmized error for each of the 140 iterations. This way it is possible to see whether exploration and exploitation are balanced. The results are evaluated by averaged error μ and success ratio SR. If the error drops sharply in the first iterations, this indicates strong exploitation, as many particles converge to and scan the promising area. In this case the search leads to a local optimum, shown by the error plateauing. This effect can be seen very clearly optimizing $f(x)$ with AIW-PSO and the parametrization of (Qin et al., 2006) with $\alpha = 0.3$ and $\beta = 1$. On the other hand, this parametrization shows a more controlled error decay for $h(x)$ and $g(x)$ compared to LDI and CIS which is also reflected by the metrics. Overall, AIW-PSO with parameters $\alpha = 0.4$ and $\beta = 10$ yields the best results; however, SR for $h(x)$ significantly decreases. This could also change with an increase in iterations, as the curves continue to decline until the last iteration. So we decided to set the iteration number to 200 for generating the training data of TAIW.

The comparison demonstrates that the strategies have a very different impact on the optimization success of the functions. Although the results of Table 3 and Table 4 cannot be directly compared due to the differing number of iterations, the trends in the curves indicate that TAIW provides the most balanced search for optimizing all functions, as there are few to no outliers. Table 4 shows the results of TAIW-PSO. Training a model instance using the training data takes approximately 2.4 minutes on a Intel Core i7-12700H CPU. The parameters (α,β) cause an inertia range of $[-3.826, 0)$ for the Rosenbrock function $h(x)$, $[-6.343, 0)$ for the Griewank function $g(x)$ and $[-39.32, 0)$ for the Rastrigin function $f(x)$.

These intervals show that the range generally increases with the risk of local optima, indicating that functions like Rastrigin, which tend to trap the algorithm, require a broader negative inertia range for enhanced exploration. Still, it is evident that the parameters of completely different loss functions are remarkably similar, indicating that this solution can be generalized across various problems. In summary, the results suggest that the neural network is able to train correlations of data structures behind the limits of the training set and finally outputs parameters for the transfer function that cause always a negative inertia for all particles. This might seem surprisingly, but during the experiments we observed notable changes in the swarm's behavior using negative inertia. The particles display a reduced tendency to get trapped in local optima. The error decreases in small steps, indicating that while the overall convergence is slower, the particles are continuously adjusting their positions and re-exploring the search space. This behavior aligns with the idea that negative inertia reverses particle direction, promoting more extensive exploration and allowing the swarm to escape local minima more effectively, without compromising the fine-grained search of promising regions.

Our work represents an initial exploration into this area, supported by empirical evidence of the negative inertia's benefits. To investigate the background further we plan to develop an optimization analysis regarding the search space probability of the different inertia strategies (see section 7).

6 MEDICAL APPLICATION

In addition to evaluating the three benchmark functions, we aim to investigate the application of PSO inertia strategies in a medical context, specifically for optimizing camera parameters in the registration process between X-ray images and digitally reconstructed radiographs (DRRs)(cf. Figure 4). The generation of digitally reconstructed radiographs (DRRs) using compute shaders in OpenGL achieves a performance of up to 940 FPS for a resolution of (256×256) on a NVIDIA GeForce RTX 3070 graphics card. A single iteration of the PSO algorithm with 1,000 particles takes 1.066 seconds. Consequently, the entire optimization process with 100 iterations requires approximately 1.8 minutes. In this study, we use a custom-built camera model designed for optimizing this registration problem. The camera, which generates the DRRs is modeled as a virtual emitter and positioned in spherical coordinates around the CT scan. The parameters $(\theta, \phi, radius, shiftX, shiftY, \gamma)$ correspond to the angular orientation and positional shifts (in millimeters) of the virtual X-ray emitter relative to the CT scan. While a detailed description of this camera model will be provided in a future publication, these parameters allow us to optimize the registration process within the framework of PSO, serving as the primary search space parametrization for this application. The parameter space examined by the PSO in this study has the following dimensions: $\theta \in [1.22, 1.7]$, $\phi \in [1.4, 1.7]$, $radius \in [350, 472]$, $shiftX \in [-10, 20]$, $shiftY \in [-10, 20]$ and $\gamma \in [1.5, 1.7]$.

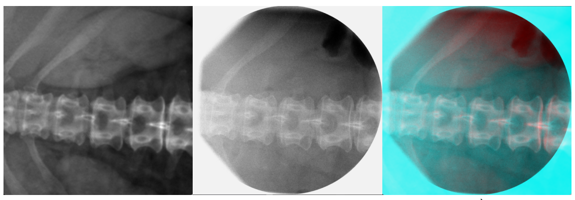

Figure 4: Registered images DRR (a), X-ray (b) and their superimposition(c) where a) is red, and b) cyan.

The metric used as an objective function is a feature-based comparison between DRR and X-ray and is not discussed in depth in this paper. It is important to note that a sufficiently accurate pose is classified as having a metric value below 27. Since the vertebrae look very similar, the registration could be shifted by one vertebra. Therefore, different poses can be classified as acceptable. Furthermore the number of iterations for this application is set to 100 due to time constraints. The network architecture remains consistent with the description in Section 4.

Figure 5 shows the results of the inertia strategies CIS, LDI, AIW (with the proposed parameters by

Table 6: Statistics of emitter parameters: θ, ϕ, γ are angles (in radians), and *radius* (r), *shiftX* (sX) and *shiftY* (sY) are shifts (in millimeters).

Model	Variance of Axes					
	θ	ϕ	r	sX	sY	γ
TAIW	0.02	0.0009	87	12	68	0.0005
CIS	0.022	0.001	154	15	72	0.001
LDI	0.014	0.002	252	21	60	0.002
AIW	0.009	0.001	116	17	20	0.001

Table 7: Statistics of the metric values for different inertia strategies TAIW, CIS, LDI and AIW.

Model	Metric	
	Mean	σ^2
TAIW	26.802	1.042
CIS	27.660	1.165
LDI	28.056	1.806
AIW	28.896	1.053

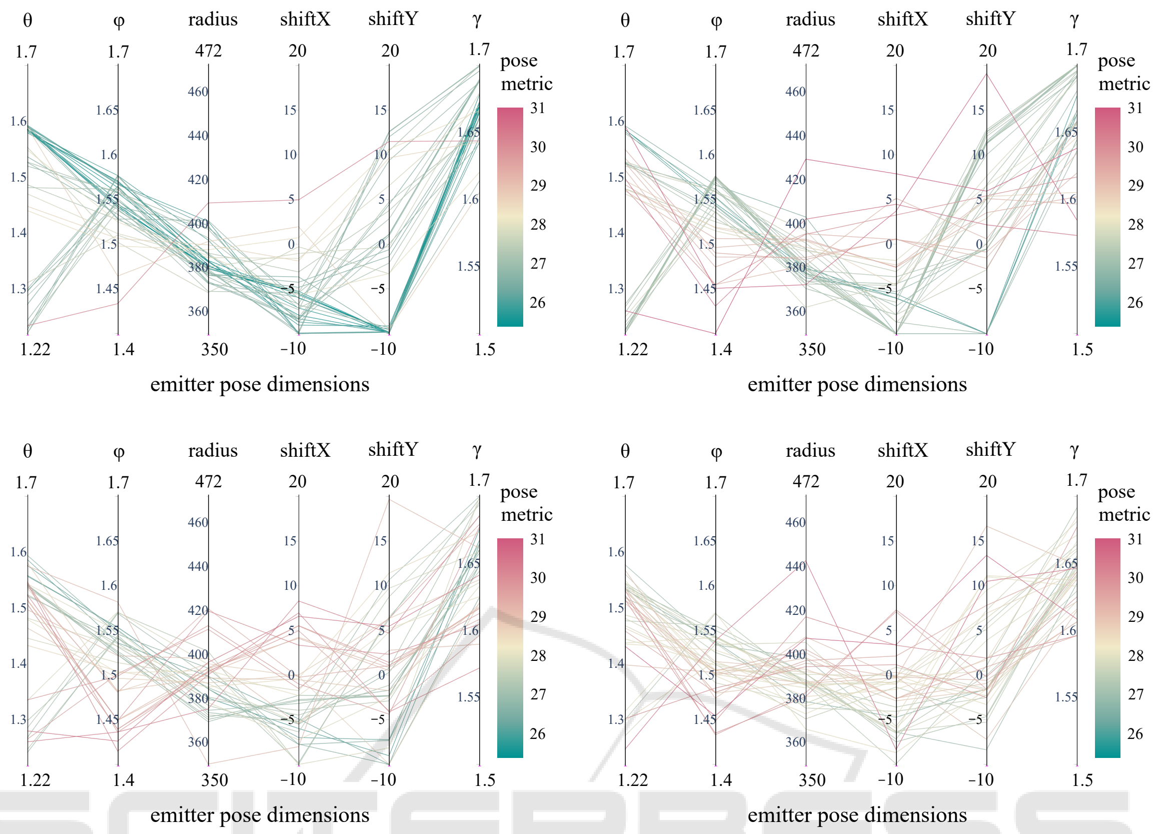

Figure 5: Visualization of the final pose results from 40 runs using the respective inertia strategy: (TAWI (upper left), CIS (upper right), LDI (lower left), AIW (lower right)); The color coding indicates the quality of the results, with red representing very poor outcomes and green representing very good outcomes.

(Qin et al., 2006)) and TAIW, respectively. The parallel plots show six axes, one for each emitter pose dimension of the virtual X-ray (DRR). They are scaled to the initial start parameter space to make the values between the PSO strategies comparable. The best poses found by PSO in each of the 40 runs are plotted for each strategy. The metric values range from a minimum of 25.38 (green) to a maximum of 31 (red). The variances presented in Table 6 correspond to Figure 5. These variances vary between axes due to differences in their physical units (e.g., angles versus millimeter shifts). Therefore, only variances within the same axis are directly comparable. Table 7 shows the strategy specific error metric mean and metric variance values, also corresponding to Figure 5.

TAIW not only achieves the lowest average metric error value across all tested approaches, but it also exhibits the smallest metric variance, which indicates a high level of consistency in performance. The color coding of the result quality based on the metric values shows that TAIW consistently produces the best results.

Furthermore, an ANOVA (Miller Jr, 1997) was performed to compare the performance of the four methods, with the methods as the independent variable and the metric values of all runs as the dependent variable. A difference is regarded as significant if $p < 0.05$. The results revealed a significant difference between the methods ($F = 21.67, p < 0.0001$), indicating that at least one method outperforms the others. Further analysis using Tukey's HSD test (Abdi and Williams, 2010) showed that TAIW significantly outperforms AIW, with a mean difference of 1.987 ($p = 0$). Additionally, TAIW also showed significant improvements over CIS and LDI, with mean differences of 0.8579 ($p = 0.0045$) and 1.2545 ($p = 0$), respectively. On the other hand, AIW was found to perform worse than both CIS and LDI, with significant mean differences of -1.1291 ($p = 0.0001$) and -0.7325 ($p = 0.0212$), respectively. No significant difference was observed between CIS and LDI ($p = 0.3951$), suggesting that these two methods perform similarly. These results highlight that TAIW provides a significant performance improvement over the other methods, particularly AIW, and reinforces the potential advantages of the TAIW approach.

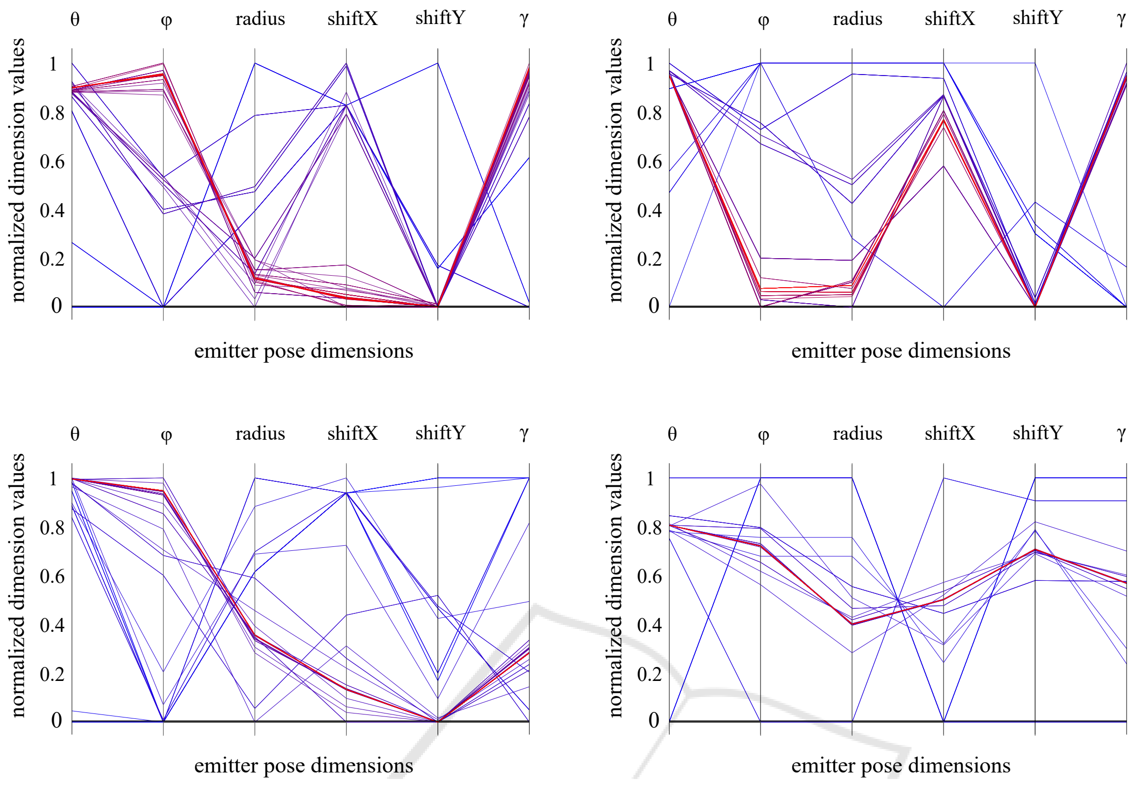

Figure 6: Visualization of the solution pose development for one PSO run using the respective inertia strategy; color coding: blue represents the first iteration, red the final iteration, with intermediate colors interpolated per iteration (TAWI (upper left), CIS (upper right), LDI (lower left), AIW (lower right)); values are normalized over all iterations; the best run is depicted for every inertia strategy.

The plots in Figure 6 show the iteration progression for one specific run for each strategy. For this purpose one specific run was selected, where the metric value is at its best to analyze how the searches lead to their best results. Iteration 1 is colored in blue and iteration 100 is colored in red. In between the iterations' colors interpolate between blue and red. The values are normalized to better highlight the color nuances of the search behavior. This allows us to observe how far the values deviate from the initial values and whether the search within those regions is uniform or more focused on specific points (helping to investigate the convergence behavior). TAIW demonstrates a metric value of 25.42, characterized by well-balanced convergence properties. Each dimension shows a smooth transition from blue to red, indicating thorough sampling across both sides of the optimum. The CIS strategy (cf. Figure 6), where the metric value is 26.1, shows similar exploration properties, as the areas around the optimum are well scanned. However, the procedure lacks the fine granularity required for targeted convergence. Therefore, the transition from blue to red can be recognized in much broader levels. Conversely, AIW has a metric value of 27.46 and reveals barely any transition, marked by an abrupt jump from blue to red, which signifies inadequate exploration. LDI strategy comes with a metric value of 25.56 and the results are similar to AIW, exhibiting strong convergence but poor exploration capabilities. To compensate for the reduced amount of training data for TAIW of only 100 training pairs, several adjustments were made. Additionally, due to time constraints, the number of runs used to calculate $\overline{\mu_e}$ and SR was reduced from 100 to 40. Although this represents a smaller sample size, it was deemed sufficient for observing consistent patterns and trends in the model's performance. The batch size was decreased from 8 to 4, allowing the model to learn more granularly from smaller subsets of data. Then, the number of training epochs was increased from 300 to 3000, ensuring the model has sufficient time to converge and extract meaningful patterns. Finally, the number of folds for the cascading cross-validation approach was increased from 5 to 10. This provides a more thorough evaluation and reduces variance in the validation process, as the model is trained and validated across a larger variety of data splits. These adjustments collectively ensure that the network generalizes well, despite the smaller dataset. The training of the loss function used for the spondylodesis application resulted in the parameters $(\alpha, \beta) = (0.72, -0.636)$. The inertia value ω remains strictly negative, falling within the range $[-1.747, 0)$ depending on the ISA value. This result closely resembles the values observed regarding the Benchmark functions, suggesting a consistent behavior across different loss functions and shows the transferability to practical medical applications.

7 OUTLOOK: OPTIMIZATION ANALYSIS

After introducing TAIW-PSO, we would like to present an outlook on a method that provides a stochastic interpretation of PSO. (Wang et al., 2018) state in their outlook that there is a lack in mathematical theory analysing the convergence behaviour. Therefore, we plan to elaborate on this method in a future paper to further investigate convergence analysis of PSO examining and comparing various strategies through a new perspective rather than solely relying on error values. For this purpose, we aim to use the n-ball hitting probability approach of (Chen and Jiang, 2010), which refers to the likelihood of randomly placing a particle into a n-dimensional space and having it intersect with a specific solution space, represented as an n-dimensional sphere. In practice, multiple solution space spheres can enclose regions of interest due to the objective function's tolerance, making it impractical to normalize the parameter scales to always describe the solution space as a sphere. Instead, we define potential solution spaces as ellipsoids, allowing the axes' lengths to vary freely across dimensions. The different PSO inertia strategies result in varied probability distributions of particle movement, leading to distinct search behaviors and, consequently, different success probabilities for intersecting with these ellipsoids. Understanding these relationships can provide insights into which strategies are most effective for specific optimization problems. Overmore, the probability of a particle encountering the solution space of the objective function is proportional to the volume of the area enclosing all particles, located in this solution space, in one iteration step averaged over multiple runs. The core idea is to cluster all particles from an iteration and use the inverse covariance matrix $\mathbf{A}$ to create ellipsoids, whose volumes can then be calculated. The definition of an ellipsoid, where $\mathbf{x}$ is an arbitrary point and $\mathbf{c}$ is the ellipsoid center is (Grötschel et al., 2012):

$$(\mathbf{x}-\mathbf{c})^{\top}\mathbf{A}(\mathbf{x}-\mathbf{c}) \leq 1 \tag{9}$$

Thus, this method has the potential providing a practical approach for calculating the n-ball hitting probability, enabling the investigation of various PSO inertia strategies' search behavior. This will help broaden comparability and yield new insights into PSO convergence analysis while reinforcing existing findings.

8 CONCLUSION

In this paper, we developed and evaluated TAIW, an extension of the AIW-PSO method, which integrates deep learning to dynamically adjust the inertia weight during the optimization process. Our approach aimed to enhance AIW by train transfer function parameters based on the individual search ability of a particle. Through extensive testing, we found that this adaptive method, driven by learned parameters, led to significantly better optimization results across various functions. A key aspect of our findings is the emergence of negative inertia as a beneficial component of the optimization process. The flexibility introduced by allowing negative inertia helped prevent the swarm from prematurely converging to local optima. This resulted in more frequent re-adjustments of the particles, allowing for a dynamic and more thorough exploration of the solution space. Our extensive tests demonstrated that TAIW consistently outperformed other methods, providing the most balanced and effective search strategy. In comparison to (Pawan et al., 2022), which limits inertia weights to positive values between 0.05 and 1, our method's ability to utilize negative inertia further underscores its flexibility and effectiveness. While our training initially started with positive inertia values, it became clear that no positive inertia could replicate the advantages observed with negative inertia. Future work could include a direct comparison of both methods to explore these differences in more detail, potentially alongside the reinforcement learning approaches.

ACKNOWLEDGEMENTS

I thank OpenAI's ChatGPT for its help refining the paper's wording. The anonymized vertebra dataset of the University of Mainz do not require ethics approval, as per Rhineland-Palatinate federal hospital law.

REFERENCES

Abdi, H. and Williams, L. J. (2010). Tukey's honestly significant difference (hsd) test. *Encyclopedia of research design*, 3(1):1–5.

Ballerini, L. (2024). Particle swarm optimization in 3d medical image registration: A systematic review. *Archives of Computational Methods in Engineering*, pages 1–8.

Bansal, J. C., Singh, P., Saraswat, M., Verma, A., Jadon, S. S., and Abraham, A. (2011). Inertia weight strategies in particle swarm optimization. In *2011 Third world congress on nature and biologically inspired computing*, pages 633–640. IEEE.

Beheshti, Z. and Shamsuddin, S. M. (2015). Non-parametric particle swarm optimization for global optimization. *Applied Soft Computing*, 28:345–359.

Bengio, Y. (2009). Learning deep architectures for ai.

Berrar, D. et al. (2019). Cross-validation.

Chen, Y.-p. and Jiang, P. (2010). Analysis of particle interaction in particle swarm optimization. *Theoretical Computer Science*, 411(21):2101–2115.

Gao, Y.-J., Shang, Q.-X., Yang, Y.-Y., Hu, R., and Qian, B. (2023). Improved particle swarm optimization algorithm combined with reinforcement learning for solving flexible job shop scheduling problem. In *International Conference on Intelligent Computing*, pages 288–298. Springer.

Grötschel, M., Lovász, L., and Schrijver, A. (2012). *Geometric algorithms and combinatorial optimization*, volume 2. Springer Science & Business Media.

Haarnoja, T., Zhou, A., Abbeel, P., and Levine, S. (2018). Soft actor-critic: Off-policy maximum entropy deep reinforcement learning with a stochastic actor. In *International conference on machine learning*, pages 1861–1870. PMLR.

Kennedy, J. and Eberhart, R. (1995). Particle swarm optimization. In *Proceedings of ICNN'95-international conference on neural networks*, volume 4, pages 1942–1948. ieee.

Kessentini, S. and Barchiesi, D. (2015). Particle swarm optimization with adaptive inertia weight. *International Journal of Machine Learning and Computing*, 5(5):368.

Kingma, D. P. (2014). Adam: A method for stochastic optimization. *arXiv preprint arXiv:1412.6980*.

Li, W., Liang, P., Sun, B., Sun, Y., and Huang, Y. (2023). Reinforcement learning-based particle swarm optimization with neighborhood differential mutation strategy. *Swarm and Evolutionary Computation*, 78:101274.

Liu, Y., Lu, H., Cheng, S., and Shi, Y. (2019). An adaptive online parameter control algorithm for particle swarm optimization based on reinforcement learning. In *2019 IEEE congress on evolutionary computation (CEC)*, pages 815–822. IEEE.

Lu, J., Guo, W., Liu, J., Zhao, R., Ding, Y., and Shi, S. (2023). An intelligent advanced classification method for tunnel-surrounding rock mass based on the particle swarm optimization least squares support vector machine. *Applied Sciences*, 13(4):2068.

Miller Jr, R. G. (1997). *Beyond ANOVA: basics of applied statistics*. CRC press.

Mirjalili, S., Song Dong, J., Lewis, A., and Sadiq, A. S. (2020). *Particle Swarm Optimization: Theory, Literature Review, and Application in Airfoil Design*, pages 167–184. Springer International Publishing, Cham.

Pawan, Y. N., Prakash, K. B., Chowdhury, S., and Hu, Y.-C. (2022). Particle swarm optimization performance improvement using deep learning techniques. *Multimedia Tools and Applications*, 81(19):27949–27968.

Qin, Z., Yu, F., Shi, Z., and Wang, Y. (2006). Adaptive inertia weight particle swarm optimization. In *Artificial Intelligence and Soft Computing–ICAISC 2006: 8th International Conference, Zakopane, Poland, June 25-29, 2006. Proceedings 8*, pages 450–459. Springer.

Shi, Y. and Eberhart, R. (1998). A modified particle swarm optimizer. In *1998 IEEE international conference on evolutionary computation proceedings. IEEE world congress on computational intelligence (Cat. No. 98TH8360)*, pages 69–73. IEEE.

Song, Y., Wu, Y., Guo, Y., Yan, R., Suganthan, P. N., Zhang, Y., Pedrycz, W., Das, S., Mallipeddi, R., Ajani, O. S., et al. (2024). Reinforcement learning-assisted evolutionary algorithm: A survey and research opportunities. *Swarm and Evolutionary Computation*, 86:101517.

Wang, D., Tan, D., and Liu, L. (2018). Particle swarm optimization algorithm: an overview. *Soft computing*, 22(2):387–408.

Yin, S., Jin, M., Lu, H., Gong, G., Mao, W., Chen, G., and Li, W. (2023). Reinforcement-learning-based parameter adaptation method for particle swarm optimization. *Complex & Intelligent Systems*, 9(5):5585–5609.

Yoon, S., Yoon, C. H., and Lee, D. (2021). Topological recovery for non-rigid 2d/3d registration of coronary artery models. *Computer methods and programs in biomedicine*, 200:105922.

Zaman, A. and Ko, S. Y. (2018). Improving the accuracy of 2d-3d registration of femur bone for bone fracture reduction robot using particle swarm optimization. In *Proceedings of the Genetic and Evolutionary Computation Conference Companion*, pages 101–102.

Zhou, J., Zhao, T., Zhao, Z., and Zheng, Z. (2024). Estimating the state of charge for lithium-ion batteries in electric vehicles using the aiw-pso-bp algorithm. In *2024 4th International Conference on Electronics, Circuits and Information Engineering (ECIE)*, pages 313–318. IEEE.